The Journal of Neuroscience, September 1, 2001, *21*(17):6967–6977

Responses of Magnocellular Neurons to Osmotic Stimulation Involves Coactivation of Excitatory and Inhibitory Input: An Experimental and Theoretical Analysis

Gareth Leng,[1] Colin H. Brown,[1] Philip M. Bull,[1] David Brown,[2] Sinead Scullion,[1] James Currie,[1] Ruth E. Blackburn-Munro,[3] Jianfeng Feng,[4] Tatsushi Onaka,[5] Joseph G. Verbalis,[3] John A. Russell,[1] and Mike Ludwig[1]

[1]Department of Biomedical Sciences, University Medical School, Edinburgh EH8 9XD, United Kingdom, [2]The Babraham Institute, Cambridge CB2 4AT, United Kingdom, [3]Department of Medicine and Physiology, Georgetown University, Washington, DC 20007, [4]School of Cognitive and Computing Sciences, University of Sussex, Brighton BN1 9QH, United Kingdom, and [5]Department of Physiology, Jichi Medical School, Minamikawachi-machi, Tochigi-ken, 329–0498, Japan

How does a neuron, challenged by an increase in synaptic input, display a response that is independent of the initial level of activity? Here we show that both oxytocin and vasopressin cells in the supraoptic nucleus of normal rats respond to intravenous infusions of hypertonic saline with gradual, linear increases in discharge rate. In hyponatremic rats, oxytocin and vasopressin cells also responded linearly to intravenous infusions of hypertonic saline but with much lower slopes. The linearity of response was surprising, given both the expected nonlinearity of neuronal behavior and the nonlinearity of the oxytocin secretory response to such infusions. We show that a simple computational model can reproduce these responses well, but only if it is assumed that hypertonic infusions coactivate excitatory and inhibitory synaptic inputs. This hypothesis was tested first by applying the $GABA_A$ antagonist bicuculline to the dendritic zone of the supraoptic nucleus by microdialysis. During local blockade of GABA inputs, the response of oxytocin cells to hypertonic infusion was greatly enhanced. We then went on to directly measure GABA release in the supraoptic nucleus during hypertonic infusion, confirming the predicted rise. Together, the results suggest that hypertonic infusions lead to coactivation of excitatory and inhibitory inputs and that this coactivation may confer appropriate characteristics on the output behavior of oxytocin cells. The nonlinearity of oxytocin secretion that accompanies the linear increase in oxytocin cell firing rate reflects frequency-facilitation of stimulus-secretion coupling at the neurohypophysis.

Key words: supraoptic nucleus; oxytocin; hyponatremia; microdialysis; hypothalamus; modeling

Neurons are nonlinear devices, but to encode information reliably over a wide dynamic range they must respond proportionately to graded stimuli and must maintain a consistent response to one stimulus during variable activation by a different stimulus. The hormones vasopressin and oxytocin, synthesized by neurons in the supraoptic and paraventricular nuclei of the hypothalamus, are released from nerve endings in the posterior pituitary. Vasopressin plays a key role in electrolyte homeostasis in mammals, and in a healthy adult, above a fixed threshold, vasopressin release increases linearly over a wide range of osmotic pressure. Thus, the relationship between the plasma concentration of vasopressin (v) and plasma osmotic pressure (x) is well characterized by the equation $v = ax + b$, where b is the "threshold" osmotic pressure or "set point," and a is the "slope" of the osmoregulatory mechanism.

In the rat, extensive studies have shown that oxytocin is also released by osmotic stimuli: acute osmotic stimuli, for instance, activate oxytocin and vasopressin cells to a similar extent, and chronic dehydration or salt loading produce similar depletion of the pituitary stores of oxytocin and vasopressin (Leng et al., 1999). Oxytocin released in response to osmotic stimuli promotes Na^+ excretion (Conrad et al., 1986; Verbalis et al., 1991) and regulates the secretion of atrial natriuretic peptide from the heart (Gutkowska et al., 1997). Although the threshold for osmotic stimulation of oxytocin release is similar to that for vasopressin, oxytocin secretion increases nonlinearly with osmotic pressure, suggesting that there are differences in the underlying osmoreceptor mechanisms. Here, we recorded the electrical activity of oxytocin and vasopressin cells *in vivo* in response to intravenous hypertonic saline and compared their behavior with a computational model. We performed similar experiments in rats made chronically hyponatremic (Verbalis, 1984), to study neuronal responses outside the normal range of osmotic pressure changes.

Both vasopressin cells and oxytocin cells of the magnocellular neurosecretory system are directly osmosensitive (Mason, 1980; Bourque, 1989; Oliet and Bourque, 1993). Osmotically induced shrinkage opens stretch-sensitive cation channels, depolarizing the cells and so increasing the probability that synaptic input (EPSPs and IPSPs) will exceed the spike threshold and trigger action potentials (spikes) (Oliet and Bourque, 1993, 1996). Much of this synaptic input arises from periventricular regions of the hypothalamus: the organum vasculosum of the lamina terminalis (OVLT), the subfornical organ, and the nucleus medianus (Nissen and Renaud, 1994). After lesions of these regions, hyperosmotic stimulation is ineffective in evoking oxytocin and vasopres-

Received March 22, 2001; revised June 4, 2001; accepted June 25, 2001.

This work was supported by grants from the European Commission, the Wellcome Trust, the Wellcome Foundation, the Medical Research Council, the National Institutes of Health (Grant DK 38094), and the Ministry of Education, Sports, Science, and Technology (Japan).

Correspondence should be addressed to Prof. Gareth Leng, Department of Biomedical Sciences, University of Edinburgh Medical School George Square, Edinburgh EH8 9XD, UK. E-mail: gareth.leng@ed.ac.uk.

 0270-6474/01/216967-11$15.00/0

sin release (Thrasher et al., 1982; Sladek and Johnson, 1983; Johnson, 1985; Leng et al., 1989; McKinley et al., 1992). These inputs are also modulated by osmotic pressure (Nissen et al., 1993), and the osmoresponsiveness of oxytocin and vasopressin cells is thus believed to be the result of a cascade of osmosensitive inputs to osmosensitive cells (Leng et al., 1982; Bourque et al., 1994).

MATERIALS AND METHODS

Electrophysiology. Male Sprague Dawley rats were anesthetized with urethane (ethyl carbamate, 1.3 gm/kg i.p.), and the trachea, a femoral, and a jugular vein were cannulated. Single cells, identified antidromically as projecting to the posterior pituitary, were recorded extracellularly from the ventrally exposed supraoptic nucleus (Leng and Dyball, 1991) with glass micropipettes filled with 0.9% NaCl. Neurons were putatively identified as vasopressin cells or oxytocin cells by their discharge patterning and by their different responses to intravenous cholecystokinin (Sigma, Dorset, UK; 20 μg/kg) (Renaud et al., 1987; Leng et al., 1991). Intravenous injections were administered via a cannula in the left femoral vein. After recording >10 min of basal activity after identification, 1 or 2 M NaCl was infused intravenously at 26–52 μl/min for 30–80 min. Blood samples were withdrawn to measure plasma [Na^+] before and after infusions.

Microdialysis. A U-shaped microdialysis probe, placed flat on the surface of the supraoptic nucleus, was used for local administration of the $GABA_A$ antagonist bicuculline (Sigma). Drugs administered in this way penetrate only a short distance into the brain—the concentrations achieved 0.5–1 mm below the surface are approximately four orders of magnitude below the dialysate concentration (in these experiments 2 mM) over this duration of infusion (Ludwig and Leng, 1997). Randle et al. (1986) quote 1.4 μM as the concentration of bicuculline necessary for 50% inhibition of GABA-mediated IPSPs in magnocellular neurons, so the dose administered by dialysis was expected to produce concentrations at the low end of the effective range within the supraoptic nucleus, but were unlikely to be effective outside the nucleus. A concentric bipolar stimulating electrode placed on the OVLT was used to evoke transsynaptic inhibition (1 Hz stimuli, matched biphasic 1 msec pulses, 0.03–0.3 mA), and 2 M NaCl was infused through a femoral vein at 26 μl/min before and after retrodialysis of bicuculline.

Measurement of GABA and glutamate release in the supraoptic nucleus. Male rats (Wistar; 300–400 gm body weight) were anesthetized with urethane (1.25 gm/kg, i.p.) and tracheotomized, and the right supraoptic nucleus was exposed by a ventral approach. A microdialysis probe (CUP11; 0.25 mm outer diameter, 1 mm length membrane) was lowered into the exposed supraoptic nucleus so that the dialysis membrane was fully inserted into the brain. Ringer's solution (in mM: 138 NaCl, 5 KCl, 1.5 $CaCl_2$, 1 $MgCl_2$, 11 $NaHCO_3$, and 1 NaH_2PO_4) was given through the probe at 1.2 μl/min using a pump (ESP-64; Eicom, Tokyo, Japan), and 20 min samples were collected from the outflow using a microfraction collector (model EFC-82; Eicom, Kyoto, Japan) at 4°C, starting 5 hr after insertion of the probe. After collecting four samples (80 min), intravenous infusion of 2 M NaCl (or isotonic saline) was started via a cannula inserted into the femoral vein at 24 μl/min for 180 min. At the end of each experiment, high K^+ solution (50 mM) was perfused into the supraoptic nucleus for 20 min to verify that the probe was effective in measuring depolarization-induced transmitter release. Concentrations of glutamic acid and GABA in the dialysate were measured by reverse phase HPLC with a fluorescence detector (model 121; 340 nm excitation and 445 nm emission filters; Gilson, Middleton, WI) after derivation with *O*-phtalaldehyde(OPA)/2-mercaptoethanol reagent. A binary methanol gradient was run with two pumps (EP-300; Eicom) (A = 50 mM phosphate buffer containing 30% methanol and 5 mg/l EDTA, pH 6.0, and B = 50 mM phosphate buffer containing 80% methanol and 5 mg/l EDTA, pH 3.5). The gradient started at 0% B, at 3 min, rose linearly to 100% during the next 3 min, maintained at 100% B for 20 min, and returned to 0% B during the next 3 min, with a flow rate of 1 ml/min. Twenty microliters of sample was automatically derivatized by incubation for 5 min at 25°C with 10 μl of 10 mM OPA, pH 9.5, by an autoinjector (model 231XL; Gilson) and applied to a C18 reversed phase column (4.6 × 150 mm; Eicopak MA-5ODS; Eicom). The column and gradient elution profile reliably separates glutamic acid and GABA from other amino acids. For data analysis, data for each rat were smoothed by averaging over 40 min fractions, and, to correct for differing basal levels, were expressed as a percentage of the first 40 min fraction. They are shown as means + SE, and statistical comparisons were made using nonparametric tests.

Hyponatremia. Hyponatremia was induced by a nutritionally balanced liquid diet combined with chronic systemic administration of a vasopressin agonist to induce inappropriate antidiuresis (Verbalis, 1984). A liquid rat diet formula (AIN-76; Bio Serv, Frenchtown, NJ) was dissolved in 14% dextrose (Sigma) at 0.54 gm/ml. Rats (278–421 gm) were housed individually, and the standard laboratory chow was substituted for 50 ml/d liquid diet mix, with *ad libitum* access to tap water. Two days later, for 1 d only, rats were given 70 ml of a more dilute diet (0.32 gm/ml). Osmotic minipumps (Alzet model 2002; Alza, Palo Alto, CA) were filled with 10 μg/ml Desmopressin acetate (Desmospray; Ferring Pharmaceuticals Ltd, Middlesex, UK) and implanted subcutaneously under halothane anesthesia resulting in a continuous infusion of Desmopressin at 5 ng/hr for up to 13 d. Rats were denied access to tap water alone during the infusion. After >5 d of infusion, rats were prepared for electrophysiology. The plasma [Na^+] in these (anesthetized) rats was 115.9 ± 2.3 mM, compared with 142–146.5 mM in the normal rats.

Blood sampling. All blood samples of 0.3 ml were withdrawn in urethane-anesthetized rats from the left femoral artery via a polythene cannula and heparinized. The plasma was separated by centrifugation and stored at −20° C. The blood cells were resuspended in isotonic saline (0.15 M NaCl) at the same volume as the plasma taken and returned via the left femoral vein. In some experiments, samples were taken from normonatremic and hyponatremic rats to determine plasma [Na^+] and [K^+], plasma osmolality, hematocrit, and plasma oxytocin concentration during infusion of 1 or 2 M NaCl at different rates. In these rats no acute surgery was performed other than cannulation of veins and arteries. Plasma [Na^+] and [K^+] were determined using a Corning 455 flame photometer, plasma osmolality by a Wescor 500B vapor pressure osmometer, and microhematocrit by centrifugation. Under urethane anesthesia there is little detected clearance of infused sodium into urine; in separate experiments involving cannulation of the bladder we were not able to detect any significant urinary clearance until after infusion of ~2 ml of 2 M NaCl (data not shown).

Infusion of hypertonic saline to urethane-anesthetized rats produced a rate- and concentration-dependent increase in plasma [Na^+], and plasma [K^+], and a fall in hematocrit. After infusion of 4.3 ml of 1 M NaCl over 60 min, plasma [Na^+] in normonatremic rats increased from 146 ± 0.7 mM (n = 4) to 165 ± 3.3 mM, and plasma osmolality rose in parallel from 296 ± 3.4 to 334 ± 4.2 mOsm/l. Plasma [K^+] rose from 3.3 ± 0.2 to 4 ± 0.2 mM, consistent with extensive cell shrinkage and entry of intracellular electrolytes into the extracellular fluid compartment. Hematocrit fell from 44.5 ± 1.3 to 40 ± 1%, consistent with an 11% increase in plasma volume. Hyponatremic rats showed similar changes in plasma [K^+] and hematocrit.

In both normal and hyponatremic rats, plasma [Na^+] showed a step increase by the time of the first sample (5 or 10 min after start of infusion), the size of which was related to the infusion rate and concentration of the infusate. Thereafter [Na^+] increased linearly for the duration of the infusion. After the end of infusions, the [Na^+] showed a step down that was inverse to the initial step up, and thereafter remained not significantly changed for up to a further 90 min. The initial step increase (of ~5.4 mM) and subsequent linearity of response is consistent with rapid clearance of infused sodium from blood into a much larger extravascular fluid compartment. Assuming a plasma volume of 10 ml that is not significantly changed within 10 min of infusion, then the measurements of plasma [Na^+] imply that, of the sodium infused continuously over 10 min, only ~8.6% remains in the plasma at 10 min.

Radioimmunoassay. In blood sampling experiments, normal or hyponatremic rats were anesthetized with urethane, and the left femoral artery and vein were cannulated for blood collection and the return of resuspended cells, respectively. The right femoral vein was also cannulated for the infusion of hypertonic saline (1 or 2 M NaCl). Blood samples (0.3 ml) were taken at timed intervals before, during, and after infusion; the plasma was separated in a centrifuge before being stored frozen for later measurement of oxytocin and/or electrolytes. The remaining cells were resuspended in an equivalent volume of 0.15 M NaCl and returned to the rat. The plasma concentration of oxytocin was measured in unextracted plasma samples using a specific radioimmunoassay, with antibody kindly donated by Professor T. Higuchi (Higuchi et al., 1986). Pre-iodinated oxytocin was obtained (NEX187; NEN Life Science Products, Hounslow, UK), and a standard curve (2.4–2500 pg/ml) was constructed using the fourth International oxytocin standard (National In-

stitute for Biological Standards and Control, Potters Bar, Hertfordshire, UK). All samples were measured in duplicate. The mean intra-assay coefficient of variance was 13.5 ± 2%, the interassay coefficient of variance was 16.7 ± 4%, and the assay sensitivity was 3.8 ± 0.66 pg/ml at 93 ± 1% of total binding.

Modeling. We modeled the oxytocin cell in the style of a modified "leaky integrate-and-fire model" (Tuckwell, 1988). EPSPs and IPSPs, generated randomly and independently at mean rates R_E and R_I, produce perturbations of membrane potential that decay exponentially. These summate to produce a fluctuating "membrane potential." When a fluctuation crosses a spike threshold, T, a spike is generated, followed by a relative refractory period, modeled as an abrupt, exponentially decaying increase in $t = T_0(1+ke^{-\lambda t})$ where t is the time since the last spike, T_0 is the spike threshold at rest, and k and λ are constants. The model program was implemented using Matlab software (MathWorks Ltd., Cambridge, UK). Intracellular recordings from oxytocin cells reveal EPSPs and IPSPs of 2–5 mV that last for 5–10 msec; we assumed that EPSPs and IPSPs at rest were of equal and opposite magnitude (at T_0) in the range 2–5 mV, with identical half lives of 3.5–20 msec. Oxytocin cells have resting potentials of approximately −62 mV with a spike threshold of approximately −50 mV (Bourque and Renaud, 1990), and are depolarized in direct response to hyperosmotic stimulation (Bourque and Renaud, 1990; Armstrong, 1995). *In vivo*, the peak activation (at ≈12 Hz) is attained after infusion of 2 ml of 2 M NaCl, which raises extracellular [Na^+] by ~10 mM, producing a direct depolarization *in vitro* of ≈3–5 mV. The equilibrium value for T, T_0, was thus set at 12 mV for the simulations shown, and simulations were conducted over 1 mV below to 5 mV above this level. We conducted simulations (250–25,000 sec of simulated activity for each parameter set) with parameter values systematically spanning the ranges above, restricted to output ranges (0–16 Hz) consistent with the behavior of oxytocin cells. Simulations illustrated are for $k = 5$, PSP heights, and half lives of 4 mV and 7.5 msec, except where stated otherwise. Reversal potentials for EPSPs and IPSPs were incorporated in an extended model; the reversal potential for IPSPs was set at −72 mV as estimated by Randle at al. (1986), and the reversal potential for EPSPs was set at −38 mV for all these simulations.

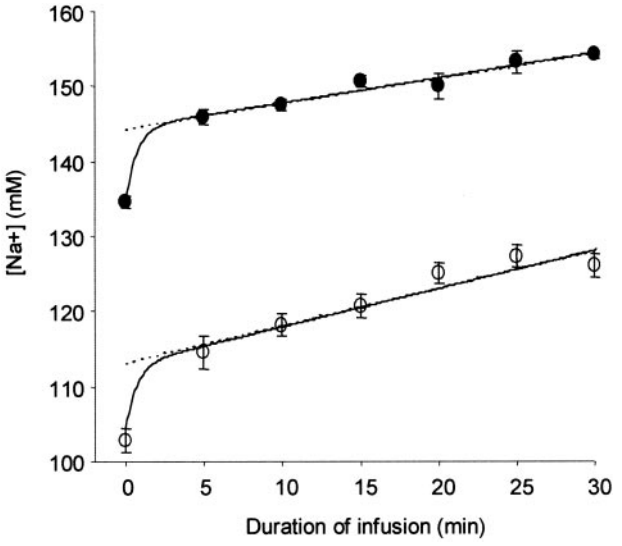

Figure 1. Sodium concentrations (± SE) in the plasma of normal rats (*closed symbols*) and hyponatremic rats (*open symbols*) during a 30 min intravenous infusion of 2 ml of 2 M NaCl. The *dashed lines* (visible only at the *left*) show best-fit linear regressions to the data between 5 and 30 min. The *solid lines* show expected plasma [Na^+] given the infusion rate, assuming that (1) [Na^+] in extracellular fluid rises linearly from the same initial values as the initial plasma [Na^+] with the same slopes as those of the regression lines shown, and (2) that Na^+ is cleared from plasma at an instantaneous rate proportional to the difference between [Na^+] in plasma and extracellular fluid, with a fixed coefficient r. The value of r was determined as 0.13 by selecting the value that best fit the data from normal rats, and this value was then applied to produce the predicted curve for hyponatremic rats.

RESULTS

In normal rats ($n = 12$), the initial plasma [Na^+] was 134.5 ± 0.8 mM. Infusion of 2 ml of 2 M NaCl over 60 min was accompanied by an increase in plasma [Na^+] to 146 ± 1 mM at 5 min, and a subsequent linear increase in concentration that was best fitted ($r^2 = 0.92$) by the equation [plasma [Na^+] (in millimolar concentration) = 144.4 (± 0.8) + 0.04 (± 0.006) × (NaCl infused in milligrams)]. In hyponatremic rats ($n = 12$) the initial plasma [Na^+] was 103 ± 1.6 mM. Infusion of the same volume of 2 M NaCl was accompanied by an increase in plasma [Na^+] to 114 ± 2.1 mM at 5 min ($n = 12$), and a subsequent linear increase in concentration that was best fitted ($r^2 = 0.88$) by the equation [plasma [Na^+] in millimolar concentration) = 113 (± 1.6) +0.07 (±0.01) × (NaCl infused in milligrams)]. Thus, the rate of increase of plasma [Na^+] was similar in hyponatremic rats to that in normal rats, and in both the rate of increase was constant after the initial step rise of ~5 mM reflecting the distribution kinetics (Fig. 1) (see Materials and Methods).

In each of 12 normal rats, an identified oxytocin cell responded to infusion of hypertonic saline with a progressive excitation that was approximately linear up to ~200 mg NaCl infused (Fig. 2). Longer recordings showed a flattening out of the response at ~12 Hz, but not all cells were recorded for long enough to confirm that this was a universal feature because, at high firing rates, the spike height was reduced, and cells became more difficult to hold in stable conditions. The initial firing rate (3.1 ± 0.7 Hz; range, 0.35–7.9 Hz) increased by 4.9 ± 0.8 Hz for the first 100 mg of NaCl infused, regardless of the rate or concentration of infusion. The response to infusion of 175 mg of NaCl was best fitted by the relationship: $y = ax + b$, where y = increase in firing rate and x = NaCl infused, for $b = -0.5 \pm 0.11$ (SE of estimate), and $a = 5.0 \pm 0.1$ Hz/100 mg NaCl infused ($r^2 = 0.99$; $n = 30$).

In each of eight normal rats, an identified vasopressin cell (initial rate, 4.5 ± 0.9 Hz; range, 0.7–8.3 Hz) was recorded during infusion of 2 M saline. Five of these cells initially showed a phasic pattern of activity previously described as characteristic of most vasopressin cells; however, all cells fired continuously throughout the infusion (Fig. 2*C*), returning to phasic activity after the end of the infusion (data not shown). Like the oxytocin cells, vasopressin cells responded to infusion of hypertonic saline with a progressive excitation that was approximately linear up to ~200 mg of NaCl infused. The response to 175 mg NaCl was best fitted by $y = ax + b$ for $b = -0.61 + 0.13$ and $a = 4.9 \pm 0.12$ Hz per 100 mg NaCl infused, values close to those for oxytocin cells ($r^2 = 0.98$; $n = 30$).

Hyponatremic rats

The plasma [Na^+] in these rats, measured under urethane anesthesia, was 115.9 ± 2.3 mM; significantly lower than in normal rats (147.7 ± 5.5 mM; $p < 0.0001$; Student's t test). In hyponatremic rats, spontaneous firing rates of supraoptic neurons (1.6 ± 0.27 Hz; $n = 46$) were on average below those in normal rats (3.8 ± 0.49 Hz; $n = 39$), but the range of spontaneous firing rates showed considerable overlap. In hyponatremic rats, no cells exhibited clear phasic activity (0 of 46 compared with 13 of 39 in normonatremic rats). Of 36 cells tested with intravenous injections of cholecystokinin (CCK), 12 showed excitatory responses similar in shape and magnitude to those characteristic of oxytocin cells in normal rats (mean change, 1.1 ± 0.32 Hz at 5 min in hyponatremic rats, compared with 1.5 ± 0.31 Hz in normal rats; $n = 13$). In normonatremic rats, phasic cells are either inhibited or unaffected

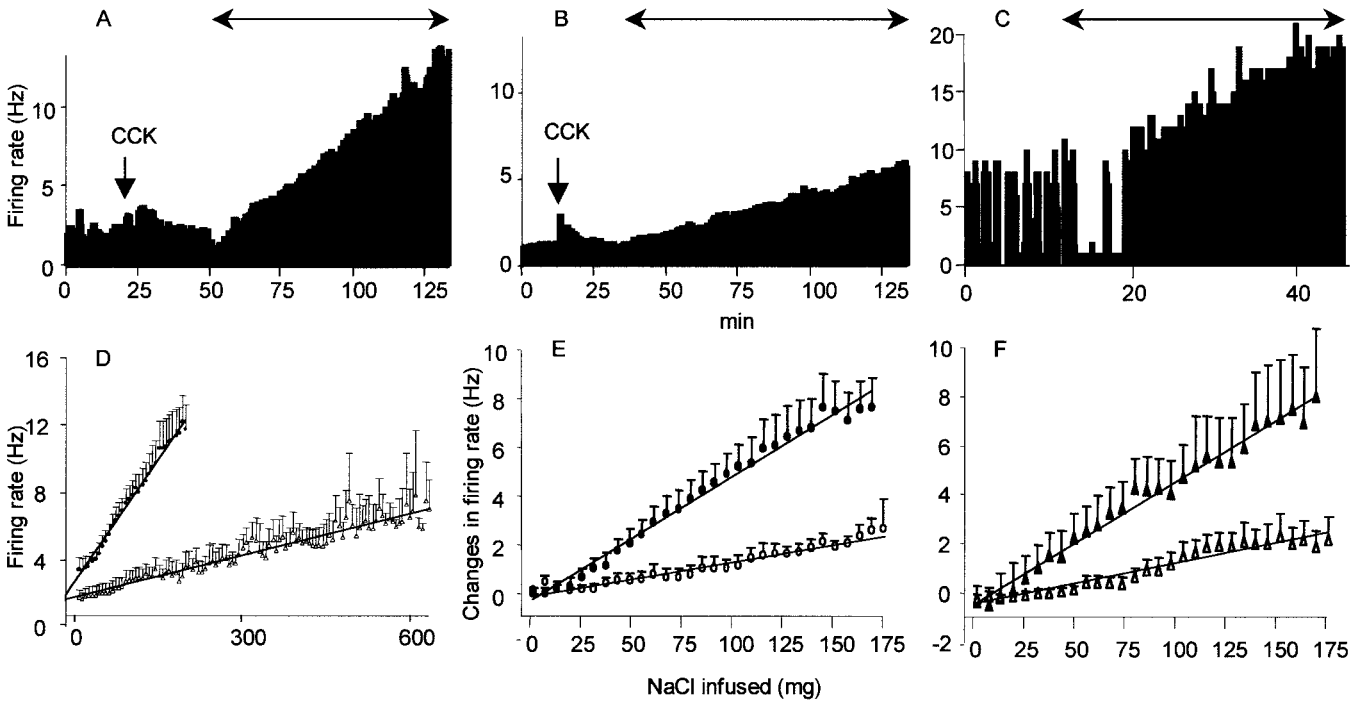

Figure 2. Responses of single oxytocin cells from a normal rat (*A*) and a hyponatremic rat (*B*) to intravenous infusion of 2 M NaCl at 26 μl/min (*double arrows*). Cells were identified by their excitatory responses to intravenous injection of CCK. The data are shown as firing rate in 30 sec bins. *C* shows data (in 10 sec bins) from a vasopressin cell in a normal rat, with characteristic phasic discharge patterning before infusion. *D–F* show average firing rates (means + SE of differences from initial firing rate). *D* shows oxytocin cells during infusion in normal rats (*closed symbols*) and hyponatremic rats (*open symbols*), with regression lines indicated. Note the linearity of the responses during infusion and the marked differences in slope between groups. Oxytocin cells (*E*) and vasopressin cells (*F*) responded linearly during intravenous infusion of hypertonic NaCl (normal rats, *closed symbols*), but with a lower slope in hyponatremic rats (*open symbols*). The lines show the linear regressions fitted to the means. (The data in *E* are a replotting of data shown in *D* and are repeated for clearer comparison with the data shown in *F*).

by CCK injection, and a minority of continuously active cells are also inhibited by CCK injection. In hyponatremic rats, of 14 cells spontaneously active at >2.5 Hz, six were excited by CCK, and five were strongly inhibited. In both normonatremic and hyponatremic rats, continuously active cells inhibited by CCK were classified as putative vasopressin cells.

Eight oxytocin cells (initial rate, 1.7 ± 0.4 Hz; range, 0.01–3.2 Hz), each in a different rat, were recorded during intravenous infusion of 2 M saline. Each responded with an increase in firing rate that was remarkably linear throughout the infusion (Fig. 2), but the slope of the response was lower than in normal rats. The response to 175 mg of NaCl was best fitted by $y = ax + b$ for $b = -0.13 \pm 0.06$ and $a = 1.4 \pm 0.06$ Hz/100 mg of NaCl infused ($r^2 = 0.98$; $n = 30$).

Six vasopressin cells (mean rate, 1.7 ± 0.7 Hz) showed a similar, weak response to infusions. The response to 175 mg of NaCl was best fitted by $y = ax + b$ for $b = -0.5 \pm 0.09$ and $a = 1.6 \pm 0.09$ Hz/100 mg NaCl infused, values close to those for oxytocin cells in hyponatremic rats ($r^2 = 0.92$; $n = 30$) (Fig. 2). Phasic firing was never observed in any cell in hyponatremic rats, even in cells recorded after infusions of hypertonic saline.

Hormone release

In parallel experiments we measured the plasma concentration of oxytocin in response to intravenous infusions of hypertonic saline. The release of oxytocin increased nonlinearly with duration of infusion (Fig. 3). This did not reflect a similar nonlinearity in the change in plasma [Na^+], which increased linearly after the initial step increase that reflects distribution kinetics (see above).

Comparing the hormone output with the observed firing rates of oxytocin cells (Fig. 3) demonstrates a strong frequency-facilitation of hormone release. Such frequency facilitation has been described previously, in experiments on the isolated neurohypophysis *in vitro*, and data from those earlier published experiments (Bicknell and Leng, 1983) are superimposed on Figure 3 for comparison. Thus, the nonlinear release of oxytocin in response to a linear increase in plasma [Na^+] results not from a nonlinearity in the cells' electrical responsiveness, but from a nonlinearity in stimulus-secretion coupling at the neurohypophysis.

Thus, oxytocin cells responded to a continuous infusion of hypertonic saline with a linear increase in continuous electrical activity over a wide dynamic range of plasma [Na^+]. We then sought to develop a concise computational model of oxytocin cells to better understand how this response is generated. We sought a model that would reproduce closely the data observed, in particular the observed patterning of spike activity, as reflected by interspike interval distributions.

Interspike interval distributions

Ten oxytocin cells and 10 vasopressin cells were selected for analysis (Fig. 4). Each interspike interval histogram was skewed, with a single mode and a long tail (Dyball and Leng, 1986); for vasopressin cells, modes were in the range of 40–60 msec, and for oxytocin cells, in the range of 30–80 msec. The tail of each interspike interval histogram (>200 msec) could be well fitted by a single exponential, and extrapolation of this exponential showed a marked deficit of intervals below the curve in the range of 0–40 msec, consistent with the effect of a hyperpolarizing

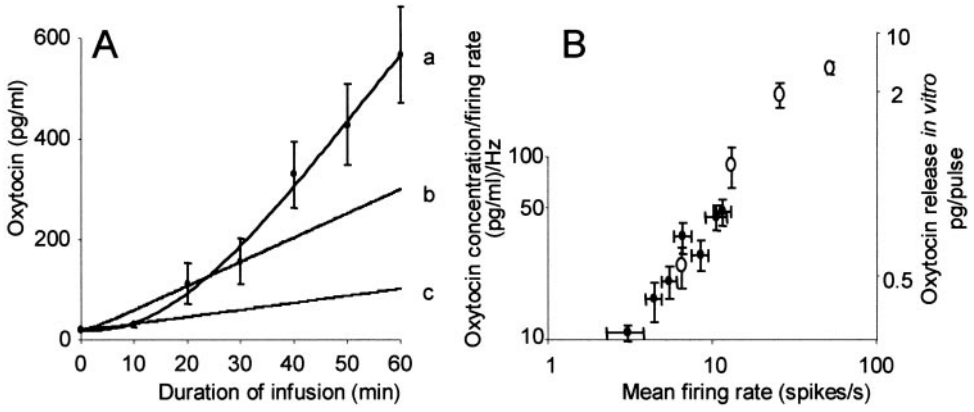

Figure 3. *A,* Oxytocin concentrations (*circles* ± SE; $n = 8–12$ per point) in plasma of normal rats during a 1 hr intravenous infusion of 2 ml of 2 M NaCl from time 0, fitted by a cubic polynomial (line *a*). The line *c* indicates the expected rise in oxytocin concentration that would accompany a basal secretion rate of 10.5 $pg \cdot ml^{-1} \cdot min^{-1}$ increasing by 2.4 $pg \cdot ml^{-1} \cdot min^{-1}$, given a constant half-life of 1.5 min. This curve was fitted to the data at time 0 and projecting a fivefold increase above the basal rate after 60 min of infusion, in line with the proportional increase in oxytocin cell firing rate. All oxytocin data after 10 min are well above this line. The line *b*, fitted to the data points at times 0 and 30 min, corresponds to a basal secretion rate of 10.5 $pg \cdot ml^{-1} \cdot min^{-1}$ increasing by 7 $pg \cdot ml^{-1} \cdot min^{-1}$. This corresponds to a 15-fold increase in secretion rate after 60 min, but still the oxytocin data at 40–60 min are above this line (and the data at 10 min are below it). Thus, in normal rats, oxytocin secretion rate increases steeply and nonlinearly during a constant infusion of hypertonic saline. *B,* Frequency facilitation of hormone release. The *closed symbols* show the mean firing rates (± SE; from Fig. 2) of oxytocin cells plotted against mean oxytocin concentrations (± SE; from Fig. 3*A*) divided by mean firing rate. Data are taken for equivalent volumes of NaCl infused intravenously and are displayed on a log–log plot. The *open symbols* show data redrawn from Bicknell and Leng (1983); these data are of oxytocin release from the isolated neurohypophysis *in vitro* in response to electrical stimulation at 6.5, 13, 26, and 52 Hz and are shown here as release rate per stimulus pulse. The *in vitro* study described frequency facilitation of oxytocin release from the neurohypophysis and shows how the release per stimulus pulse increases as the frequency of stimulation increases. For ease of comparison, the *in vitro* data were scaled so that the release rate at 6.5 Hz *in vitro* appears close to the release rate observed *in vivo* when cells are active at approximately this frequency.

afterpotential. For every vasopressin cell, there was an excess of intervals above the curve in the range of 40–100 msec, consistent with the effect of a depolarizing afterpotential. No such excess was observed in any oxytocin cell, indicating that oxytocin cells display little or no depolarizing afterpotential when normally active *in vivo*. The good exponential fits obtained for oxytocin cells suggest that, beyond ~80 msec after any given spike, the arrival time of the next spike is essentially random. This indicated that the activity of oxytocin cells is dominated by (1) factors affecting the probability of spike occurrence that are independent of previous spike history, i.e., the mean resting potential and the rate of synaptic input, and (2) a reduction in excitability following each spike that decays over 40–80 msec.

Simulating oxytocin cell activity

To test this inference, we modeled oxytocin cells by a leaky integrate-and-fire model, modified to mimic the post-spike reduction in excitability. The interspike interval histogram from each oxytocin cell could be closely matched by a model cell with a resting potential (T_0) of 12 mV below spike threshold subject to random EPSPs of 4 mV amplitude and 7.5 msec half-life, where the function describing the post-spike hyperpolarization was of the form $t = T_0(1 + ke^{-\lambda t})$, where $k = 5$, and where λ was in the range 0.08–0.15 (Fig. 5*A*). Each oxytocin cell could be closely fitted by varying just λ and R_E. The fits were not unique; good fits could be achieved for larger (smaller) values of EPSP size or half-life or for more depolarized (hyperpolarized) values for T_0 by compensatory changes in R_E. Good fits could also be achieved with different values of k by adjusting λ (data not shown). Similarly, the shape of the interspike interval histogram is little affected if the model is challenged not with EPSPs alone but with a mixture of EPSPs and IPSPs. However, for PSP parameters in the stated ranges, and for a chosen value of k, every interspike interval histogram from an oxytocin cell could be characterized by a unique λ, and by the parameters T_0, $R_{E\ and\ RI}$, which affect the output rate but have little other effect on the shape of the interspike interval histogram in the relevant range (Fig. 5*A*).

This enabled us to test the hypothesis that the oxytocin cell response to osmotic stimulation arises from an increase in synaptic input combined with a direct depolarization, with no change in the intrinsic mechanisms that govern post-spike excitability. If so, then it should be possible to fit interspike interval histograms from any one oxytocin cell at different levels of activity with a common λ. This proved true for each cell tested (Fig. 5*B*).

We then studied how the firing (output) rate of model cells changes with the synaptic input rate, and with increasing depolarization. In the absence of IPSPs, an increase in EPSP rate (R_E) produces a nonlinear increase in output, regardless of the parameter values within the stated ranges (Fig. 6*A*). We checked to see if elaborating the model to incorporate a reversal potential for EPSPs (of −38 mV) would significantly alter this conclusion; it does not (Fig. 6*B*). The effective dynamic range of oxytocin cells is from ~1 Hz (lower range of spontaneous rates) to ~10 Hz (peak sustained rates). This range was spanned in the model cells by a narrow range of R_E; in the representative examples in Figure 6*B*, by a change in R_E from 60/sec to 130–180/sec, depending on λ. Thus a 10-fold increase in output rate follows a less than threefold increase in input rate. Osmotic stimulation is accompanied by a direct depolarization of 3–5 mV, and an equivalent change in T_0 leads to a compression of the range of R_E needed. In the representative example in Figure 6*E*, an increase in R_E from 60–80/sec, accompanied by a 4 mV depolarization, produces a change in output rate from 1 to 10 Hz. Thus, under these conditions, a 10-fold increase in output rate follows an increase in input rate of ~33%. Even with no increase in input rate, the expected increase in output rate is substantial. A 4 mV depolarization alone, with R_E unchanged at 60/sec, produces an increase in output rate from 1 to 6.3 Hz. This suggests that tonically active oxytocin cells subject to EPSP input alone will respond strongly to osmotic stimuli as a result of the direct depolarizing influence of increased osmotic pressure alone, even without any change in synaptic input.

Furthermore, similar absolute changes in R_E from a different initial rate, but accompanied by the same osmotic depolarization, result in very different amplitudes of responses. For the simulations shown in Figure 6*G* we chose a range of values of R_E that resulted in output rates in the range 0.2–5 Hz, and then calculated

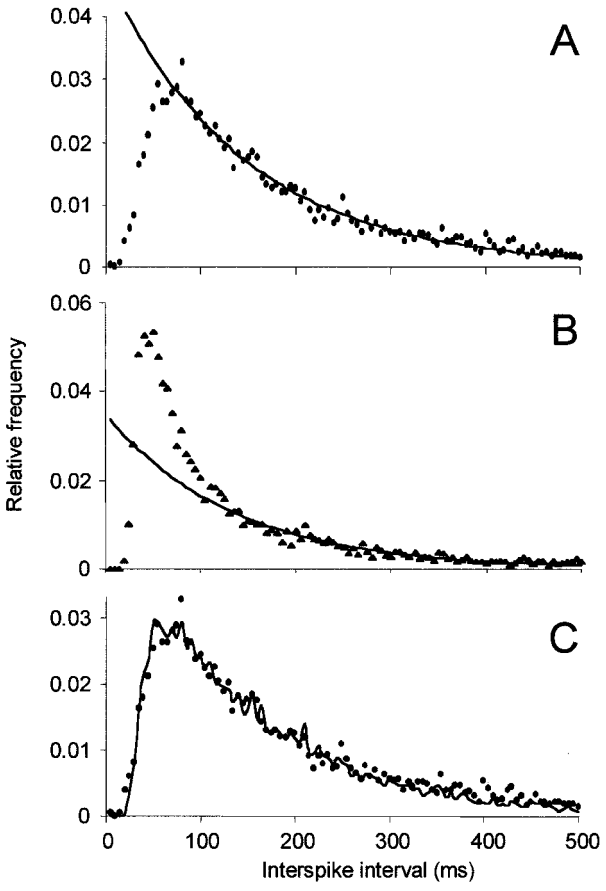

Figure 4. Representative interspike interval histograms from an oxytocin cell (*A*) and a vasopressin cell (*B*) showing exponential curves fitted to the histogram tails and extrapolated to lower interval values. For vasopressin cells, but not for oxytocin cells, such extrapolations revealed a large excess of intervals above the fitted curve in the range of 30–150 msec. *C* shows the interspike interval histogram of a model cell (*line*) superimposed on that of the oxytocin cell. This match was achieved for $\lambda = 0.08$ (other parameters as in Materials and Methods) using equal average numbers of EPSPs and IPSPs ($I_E = I_I = 380$ Hz). Model distributions were constructed from simulation of 1800 sec of activity. The mean firing rate of the oxytocin cell and the mean output rate of the model cell were both 6.0 Hz. Each interspike interval histogram is normalized to the total number of events analyzed.

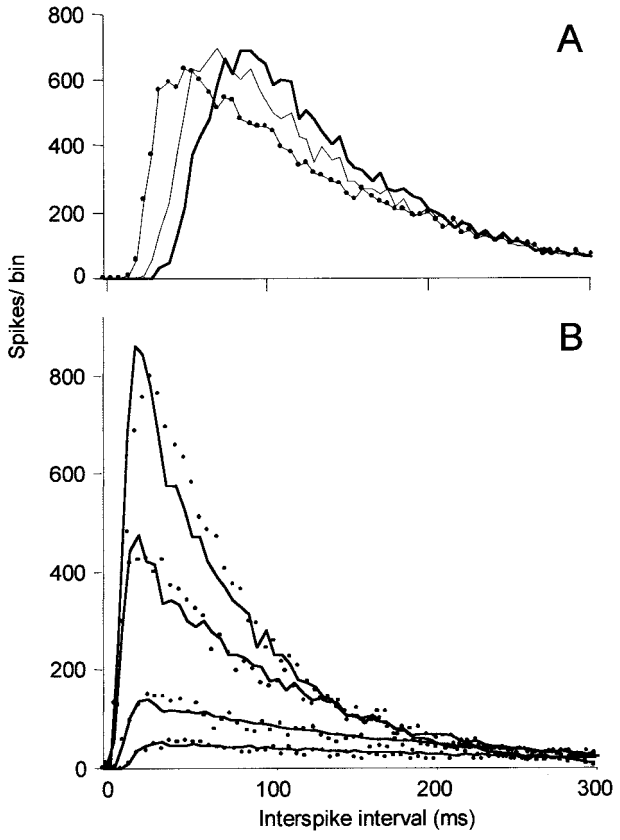

Figure 5. *A,* Increases in λ produce increasing values for the mode of the interspike interval histogram. Plotted distributions are for $\lambda = 0.1$, 0.07, and 0.05 (*bold line*); EPSP rates (I_E; 160, 168, and 172/sec, respectively) were adjusted to achieve similar output rates of 7 Hz. Each model cell interspike interval histogram is from 25,000 sec of simulated activity. *B,* Comparison between model interspike interval histograms (*lines*) at different levels of synaptic input, and interspike interval histograms observed in an oxytocin cell at different times during infusion of hypertonic saline (*points*). Oxytocin cell interspike interval histograms were constructed over 1000 sec, model cell interspike interval histograms over a simulated 25,000 sec, normalized for comparison. Oxytocin cell interspike interval histograms correspond to mean firing rates of 12.8, 9.3, 4.8, and 2.5 Hz. Model cell interspike interval histograms ($\lambda = 0.08$) were constructed for equal average numbers of EPSPs and IPSPs, over a range of PSP frequencies that matched the range in firing rates observed during the period of recording analyzed, producing output rates close to the average oxytocin cell firing rates. A single value of λ produces good fits for this cell at all levels of activity.

for each of these values, the increase in output rate that resulted from fixed incremental increases in R_E. This analysis suggests that oxytocin cells that differ in initial firing rate slightly as a result of differing initial EPSP rates will respond in a divergent manner to a subsequent identical stimulus (Fig. 6*G*).

Although these inferences are broadly independent of assumptions about EPSP size, half-life, and potential, they are not consistent with experimentally observed behavior. Osmotic stimulation is accompanied by extensive increases in the activity of afferent neurones (McKinley et al., 1992; Bourque et al., 1994). Moreover, the inference of divergent responsiveness of cells with different initial firing rates is not consistent with the linearity of the neuronal responses observed here *in vivo* or with the reproducibility of responsiveness among neurons with differing initial spontaneous firing rates. However, in model cells, the relationship between output rate and input rate becomes shallower as the ratio of IPSPs to EPSPs is increased. This is true both for models that assume that EPSP and IPSP size are independent of voltage (Fig. 6*C*) and for models that incorporate appropriate reversal potentials for both (Fig. 6*D*).

Comparing simulation results of models with and without reversal potentials, it is apparent that although the latter are less sensitive to synaptic input, it is equally true for both models that a high proportion of IPSPs produces a linearization of the input–output relationship (Feng and Brown, 1999). The model used here, with the EPSP reversal potential v_e and IPSP reversal potential v_i can be expressed by the equation:

$$dv(t) = -(\log 2/T_{\text{half}})(v(t) - v_{\text{rest}})dt + a(ve - v(t))dN(t) - b(v(t) - vi)dM(t),$$

where $v(t)$ is the membrane potential at time t; v_{rest} is the resting potential; $a(v_e - v_{rest})$ and $b(v_{rest} - v_i)$ are the magnitudes of single EPSPs and IPSPs at the resting potential; $N(t)$ and $M(t)$ are

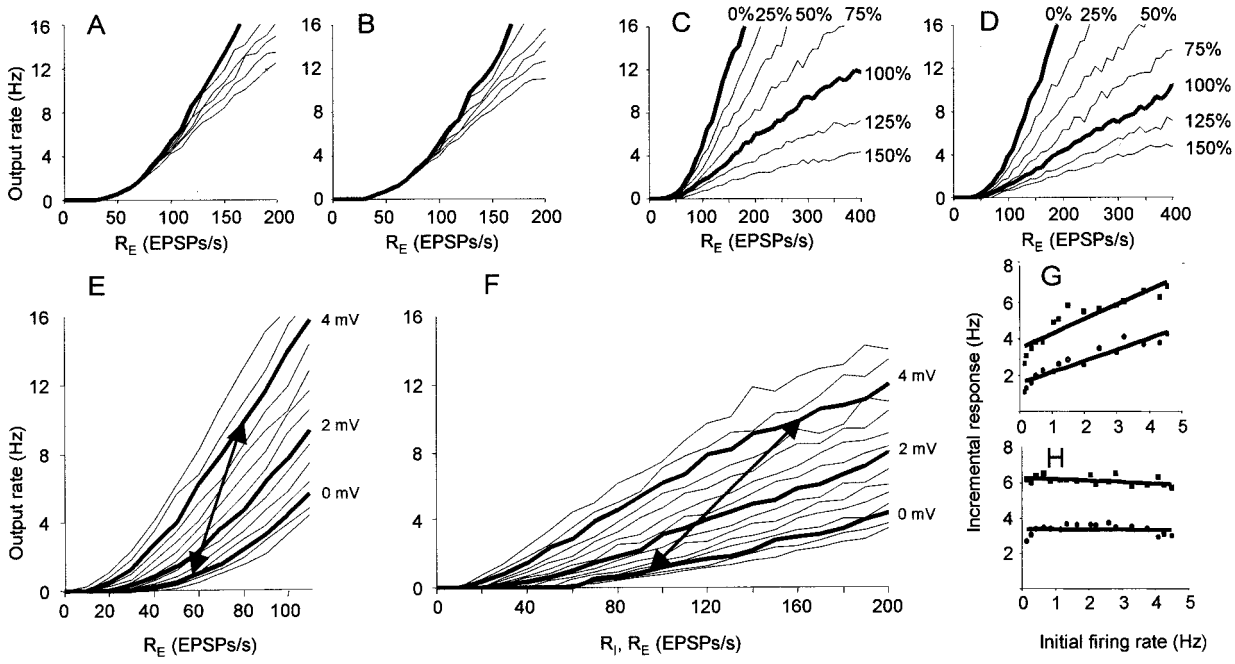

Figure 6. *A,* Relationship between model cell output rate and EPSP rate R_E for values of λ that provided close fits to the interspike interval histograms of oxytocin cells. Firing rates were calculated from simulation of 2500 sec of activity at every R_E between 0 and 200 in steps of 10 for λ = 0.14, 0.1, 0.08, 0.07, 0.06, and 0.05. Note the nonlinearity of the response to increasing R_E. *B* as for *A,* but incorporating a reversal potential of −38 mV for EPSPs. *C*, Effects of increasing proportions of IPSPs in the input; λ = 0.1. In each simulation, EPSPs are present at the rate indicated on the abscissa, and IPSPs are present at the proportional rate indicated. *D* as for *C*, but incorporating a reversal potential of −38 mV for EPSPs and −72 mV for IPSPs. *E, F,* Relationship between output rate and R_E in models that incorporate reversal potentials as above (λ = 0.1), and values of resting potential vary in 0.4 mV steps above and below the standard value used for simulations (*line marked 0 mV*), corresponding to −62 mV, 12 mV below spike threshold (−50 mV). The *double-headed arrows* connect points corresponding to an output rate of 1 Hz at the initial resting potential to points corresponding to 10 Hz at a membrane potential depolarized by 4 mV. This line thus indicates the apparent dynamic range of oxytocin cells in response to osmotic stimulation *in vivo*. *E* shows simulations for a cell stimulated by EPSPs alone, and *F* shows simulations for a cell stimulated by an equal number of EPSPs and IPSPs. *G* and *H* display the same model cell responses to a fixed increment in PSP rate combined with a depolarization of 4 mV from a resting potential 12 mV below spike threshold. *G* shows responses of cells with EPSP input alone to increments of 4/sec (*circles*) or 8/sec (*squares*) from initial EPSP rates of 48–170/sec (chosen to produce firing rates in the model cell in the range of 0–5 Hz). *H* shows responses of cells with balanced EPSP–IPSP input to increments of 64/sec (*circles*) or 128/sec (*squares*) from initial PSP rates of 72–336/sec. With EPSP input alone, the size of the response depends on the initial firing rate and is sensitive to small changes in R_E. With balanced input, the size of the response is mainly independent of initial firing rate and requires a larger proportionate change in input rate. The lines in *G* and *H* show the linear regression fits to the data shown. Graphs are constructed from simulations of 2500 sec of activity for each point plotted.

Poisson processes with rate R_E and R_I respectively; and T_{half} is the half life of EPSP and IPSPs. This can be rewritten as:

$$dv(t) = -[(\log 2/T_{\text{half}})dt + adN(t) + bdM(t)](v(t) - v_{\text{rest}}) + a(ve - vrest)dN(t) - b(vrest - vi)dM(t).$$

When written in this form, we see that there are three "leakage" terms: $(\log 2/T_{half})\ (v(t) - v_{rest})dt$; $a(v(t) - v_{rest})\ dN(t)$; and $b(v(t) - v_{rest})dM(t)$. Without the second and the third leakage terms, we obtain the model without reversal potentials. Hence, incorporating reversal potentials reduces the effective half-life of single EPSPs and IPSPs compared with the model without reversal potentials. The higher the input frequency is, the stronger the reduction. Comparing Figure 6, *A* with *B* and *C* with *D,* reveals the impact of this: a (relatively modest) attenuation of the slope of the input–output relationship. Including reversal potentials enhances the linearizing effect of IPSPs on the input–output characteristics of the model neuron, and this is true generally, not just for the particular parameters used here for illustration.

We therefore conducted simulations combining a direct depolarization with an increase in balanced input, comprising equal average numbers of EPSPs and IPSPs. For the example in Figure 6*F*, a change from 1 to 10 Hz accompanied by a 4 mV depolarization requires an increase in R_E and R_I from ~94/sec to ~164/sec; a 74% increase in input rate, rather than the 33% increase in input rate required of the same model cell challenged with EPSPs alone (Fig. 6*E*). Importantly, model cells that differ in initial output rate as a result of differing initial input rates respond similarly to a given stimulus (Fig. 6*H*).

Testing model predictions

We blocked $GABA_A$ receptors with the antagonist bicuculline, delivered to the dendritic zone of the supraoptic nucleus, while recording the response of oxytocin cells to osmotic stimulation (Fig. 7), having previously shown that this dose and route of application of bicuculline is effective in blocking both the actions of muscimol applied by microdialysis and the inhibition induced by stimulation of the arcuate nucleus (Ludwig and Leng, 2000).

To establish the efficacy of bicuculline, a stimulating electrode was placed in the OVLT. As described elsewhere (Yang et al., 1994), OVLT stimulation activates monosynaptic projections to the supraoptic nucleus that are in part inhibitory and in part excitatory, and also has polysynaptic effects via the projection from the OVLT to the nucleus medianus. However, most supraoptic cells display a clear short-latency inhibition after OVLT stimulation, and in some only inhibition is seen, as in the cell

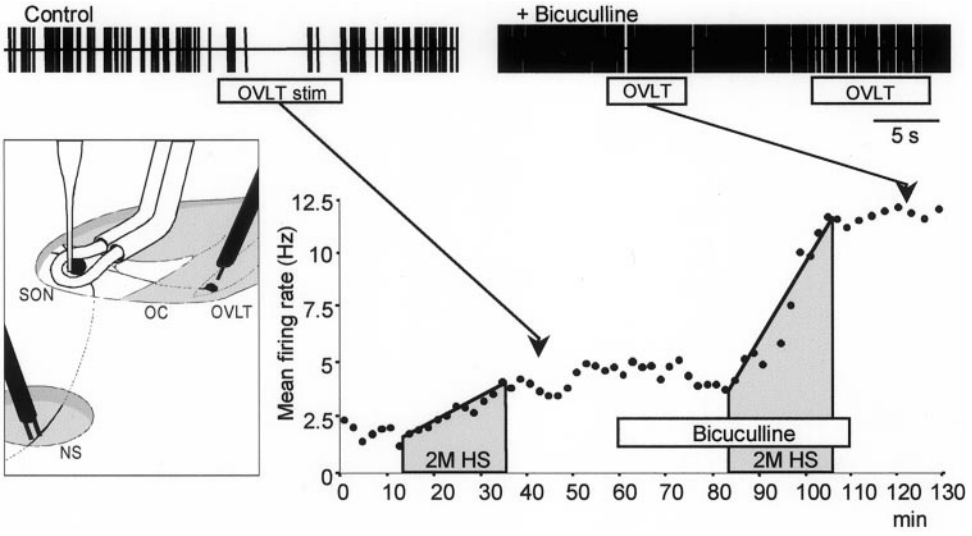

Figure 7. A microdialysis probe was placed on the surface of the supraoptic nucleus for local drug administration while recording the electrical activity of single oxytocin cells. *Top,* The bars mark periods of stimulation of the OVLT below event marker records of spike discharge in an oxytocin cell. The inhibitory response to stimulation was blocked during dialysis with bicuculline (*right traces*). *Bottom,* Firing rate of the same cell in 1 min bins. Slow intravenous infusion of 2 M NaCl (HS) produces the expected increase in discharge rate before bicuculline but a much greater increase during bicuculline. OVLT stimulation was applied at the periods marked.

illustrated in Figure 7. In this cell, and in cells thus tested, the trans-synaptic inhibition evoked by stimuli applied to the OVLT was blocked during dialysis with bicuculline. In this experiment, hypertonic saline was infused intravenously for 10 min before bicuculline, and the cell showed the expected linear increase in discharge rate. The same stimulus repeated after 25 min infusion of bicuculline produced a much steeper response. This experiment was repeated for five oxytocin cells, each in a different rat, and all showed an enhanced rate of response in the presence of bicuculline (Fig. 8) (mean increase in average rate of response: 83%; range, 24–206%). The steeper response was not a delayed response to bicuculline: continuous infusions of bicuculline alone, in separate experiments without osmotic stimulation, produced a small increase in discharge rate that was maximal within 10 min and that was sustained for up to 40 min after the end of infusion (Ludwig and Leng, 2000).

We considered whether a similar change in response slope would be expected from attenuation of a tonic GABA input, rather than an input that increases during hypertonic infusion, or from a removal of a shunting influence of a tonic GABA input with the equivalent effect of increasing EPSP size. In model simulations, the effect of either of these would be a leftward shift in the relationship between EPSP frequency and model output, but with little effect on slope (data not shown). Thus, blocking a tonic input or removing a tonic shunting influence equivalent to a 20% increase in EPSP size would be expected to be reflected in the neuronal response to bicuculline alone, with no substantial effect on responsiveness to osmotic stimuli at least for firing rates >3 Hz.

Measurement of GABA release in the supraoptic nucleus

Finally, we tested directly the inference that hyperosmotic stimulation induces GABA release in the supraoptic nucleus. We measured concentrations of GABA and glutamate in fractions of dialysate collected from the supraoptic nucleus during intravenous infusion of hypertonic saline, as above. In control rats, intravenous infusion of isotonic saline produced no significant change in release of either GABA or glutamate. In rats infused with hypertonic saline there was, as expected, a significant and approximately linear increase in glutamate concentration measured over 2 hr of infusion, and as predicted, a similar increase in GABA concentration (Fig. 9).

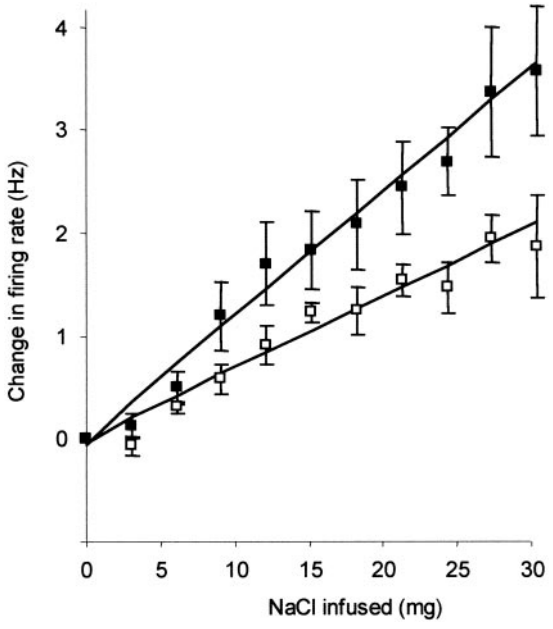

Figure 8. Average change in firing rate of five oxytocin neurons from normal rats during microdialysis with aCSF (*open symbols*) and bicuculline (*closed symbols*), in response to intravenous infusion of 2 M NaCl. The points are means ± SE of differences from the firing rate at the start of infusion, and the lines show the linear regressions fitted to the means. The control response to infusion was best fitted by the relationship: $y = ax + b$, where y = increase in firing rate and x = NaCl infused, for $b = -0.05 \pm 0.07$ (SE of estimate) and $a = 6.9 \pm 0.5$ Hz/100 mg NaCl infused ($r^2 = 0.98$). The response in the presence of bicuculline was best fitted for $b = -0.06 \pm 0.09$ and $a = 12.0 \pm 0.5$ Hz/100 mg NaCl infused ($r^2 = 0.95$).

DISCUSSION

These experiments were designed to address the hypotheses that the apparent set point for osmoregulated hormone secretion reflects a fixed set point for osmotic activation of oxytocin and vasopressin cells and that vasopressin cells respond linearly, whereas oxytocin cells respond nonlinearly. Both hypotheses must be discarded. In hyponatremic rats, the discharge activity of oxytocin cells is regulated by osmotic pressure over a range well below the normal set point for oxytocin release. Moreover, the linear regression fits of firing rates in response to hypertonic

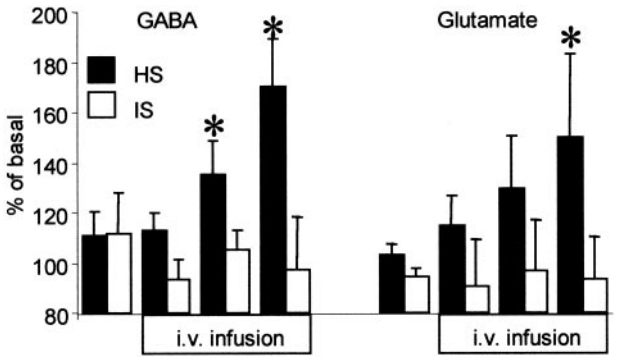

Figure 9. GABA and glutamate concentrations in fractions of dialysate collected from microdialysis of the supraoptic nucleus during intravenous infusion of hypertonic saline (2 M NaCl at 26 μl/min; $n = 6$) or isotonic saline ($n = 4$). Values are means + SE of data expressed as a percentage of control (mean preinfusion) values for each rat.

infusions show no difference in the slope of the response between oxytocin cells and vasopressin cells in either normal rats or hyponatremic rats, indicating no differences between the cell types in the fundamental mechanisms of osmoresponsiveness. In hyponatremic rats, the intercepts of the regression lines of the responses were close to zero, indicating no apparent threshold of osmoresponsiveness for either cell type. However, the slopes were more shallow in hyponatremic rats. The difference in slope did not simply reflect the lower initial firing rate of cells in hyponatremic rats, because no change in slope was observed once firing rates reached the range observed in normal rats (Fig. 2*D*). Thus, the attenuated slope of osmotic responsiveness reflects a fundamental change or adaptation in responsiveness in hyponatremia. The underlying mechanisms are not known, but although the acute response of neurons to hyponatremia is a volume expansion, in the chronic hyponatremic state, the cells are hypotrophied (Zhang et al., 2001). It seems possible that the expression of stretch-inactivated channels that underlie direct osmoresponsiveness (Oliet and Bourque, 1993, 1996) is downregulated in this chronic condition, as shown for other genes (Glasgow et al., 2000). It is also possible that the reduced extracellular [Na^+] may affect the behavior of these channels (Voisin et al., 1999).

Hypertonic saline infusion also induces hypervolemia and an increase in plasma [K^+]. The release of oxytocin and vasopressin is potently stimulated by volume reductions in excess of 25% (Stricker and Verbalis 1986), so we should consider whether hypervolemia may have attenuated the neuronal response to hyperosmolality. This seems unlikely, because decreases of plasma volume of <5% have no significant effect on the secretion of either vasopressin or oxytocin in the rat (Stricker and Verbalis 1986), but there are interactive effects between the stimuli. However, we can compare the responses of oxytocin cells to hypertonic infusions with the responses to intraperitoneal injection of hypertonic saline, a stimulus that induces a modest hypovolemia rather than modest hypervolemia. Intraperitoneal injection of 1 ml of 1.5 M NaCl increases plasma [Na^+] by ~8 mol/l over 20 min and increases the discharge rate of supraoptic neurons by ~2 Hz (Shibuki et al., 1988; Leng et al., 1989). In the present study, the firing rate of supraoptic neurons increased by 5 Hz/100 mg of NaCl infused, and plasma [Na^+] by 7 mol/l per 100 mg of NaCl infused. Clearly, intravenous hypertonic infusion is accompanied by a larger rate of increase in firing rate seen after intraperitoneal injection of hypertonic saline, and not a lower rate as would be expected if the hypervolemic and hyperkalemic components had a significant attenuating effect.

Previous studies have reported that osmotic challenge to hyponatremic rats induces c-*fos* expression but no significant hormone release (Ivanyi et al., 1995). The present studies demonstrate that oxytocin cells in hyponatremic rats increase their firing rate in response to hypertonic infusion, but from lower basal firing rates than in normal rats, and more gradually. Oxytocin secretion increases nonlinearly as discharge rate increases, and low levels of activity are relatively ineffective in releasing oxytocin (Fig. 3). The apparent set point for oxytocin release thus reflects a discharge activity in excess of that necessary for significant secretion to occur, rather than an absolute threshold for cell activation.

The linearity of the cell response over a wide dynamic range was surprising, but the modeling suggested that this could be well explained if hypertonic infusion produces a coactivation of excitatory and inhibitory inputs. The OVLT is the source of both excitatory and inhibitory inputs to the supraoptic nucleus; the inhibitory component is GABAergic, and may be directed mainly to vasopressin cells (Yang et al., 1994). Studies *in vitro* suggest that only the excitatory input is activated directly by osmotic stimulation (Richard and Bourque, 1995).

However the OVLT projects extensively to the nucleus medianus, and neurons in this region are activated by systemic osmotic stimulation, apparently via the projection from the OVLT. The experiments of Richard and Bourque (1995) involved applying hyperosmotic solution specifically to the OVLT in an explant preparation in which the nucleus medianus is not intact. The results exclude any involvement of direct GABA inputs from the OVLT in the osmotic responses of supraoptic neurons, but the authors nonetheless state that "inhibitory inputs from the [nucleus medianus] may indeed participate in the osmotic control of magnocellular neurosecretory cells."

Stimulation of the nucleus medianus, by electrical stimulation or by local application of glutamate, mainly inhibits magnocellular neurons, probably through $GABA_A$ receptors because the inhibition can be blocked by bicuculline (Nissen and Renaud, 1994). Approximately two-thirds of nucleus medianus neurons that project to the supraoptic nucleus are activated by systemic osmotic stimulation (Aradachi et al., 1996). It seems likely therefore that nucleus medianus neurons are the source of the increased GABA release measured in these experiments. However, in the first experiments that reported the direct depolarizing effects of hypertonic solutions on oxytocin and vasopressin cells (Mason, 1980), an increase in IPSP frequency was also described, and in this preparation only local inputs from the perinuclear zone were preserved.

It is natural to assume that an increase in neuronal firing rate implies an increase in excitatory input and/or a direct depolarization. However, where PSP sizes are relatively large, as for magnocellular neurons, an increase in firing rate will occur in response to an increase in excitatory input even when there is an accompanying, balancing increase in inhibitory input. As we show here, when cells are subject to an increase in balanced input, the response is more linear and shallow than when cells are subject to an increase in excitatory input alone.

The present oxytocin cell model indicates that an increase in IPSP frequency that accompanies either an increase in EPSP frequency or a steady depolarization will moderate the rate of increase in firing rate, will linearize the input–output relation-

ship, will extend the effective dynamic range of the output neuron, and will tend to make the response of a neuron to a given input independent of the initial firing rate. The present work indicates that a high proportional activation of inhibitory input confers appropriate characteristics on the responses of magnocellular neurons to osmotic inputs, and thus assigns an important functional relevance to inhibitory pathways from periventricular structures to the magnocellular system.

The responses of vasopressin cells to hypertonic infusions were similar to those of oxytocin cells, despite differences in electrophysiological properties of the two cell types. The most conspicuous difference is that vasopressin cells, unlike oxytocin cells, normally discharge phasically; phasic firing reflects in part a depolarizing afterpotential, the impact of which is evident in the comparisons of interspike interval distributions between oxytocin and vasopressin cells (Fig. 4). However, in response to gradually escalating input, phasic firing is not generally observed; for instance after intraperitoneal hypertonic saline, vasopressin cells normally respond by continuous firing that only breaks up into phasic firing once a new equilibrium is established (Brimble and Dyball, 1977). Similarly in these experiments, vasopressin cells fired continuously during intravenous hypertonic infusions, although after termination of the infusion some resumed phasic firing. Because the depolarizing afterpotential is subject to activity-dependent inactivation (Leng et al., 1999), it is perhaps not surprising that vasopressin cells respond like oxytocin cells in conditions in which vasopressin cells fire continuously and in which the depolarizing afterpotential may be inactivated.

During hypertonic infusions, vasopressin cells fired continuously rather than in the phasic pattern that optimizes the efficiency of vasopressin release. As shown by Stricker and Verbalis (1986), in the acute phase after intraperitoneal injection of hypertonic saline, much more oxytocin is secreted than vasopressin, whereas in the chronic phase the secretion of vasopressin is more sustained. Whether this is of physiological significance is questionable; the continuous firing in vasopressin cells may simply reflect the response to stimulation that is progressively increasing at a rate that exceeds any seen under normal physiological conditions. As observed elsewhere (Leng and Brown 1997), phasic discharge has features that suggest that vasopressin cells behave as bistable oscillators. Phasic bursts are maintained by activity-dependent plateau potentials, and cells achieve an unstable equilibrium when (relatively fast) activity-dependent reactivation of the plateau is balanced by (relatively slow) activity-dependent inactivation. When synaptic input and direct depolarization are increasing progressively, activation will always exceed inactivation, and the equilibrium state that is a prelude to oscillations will not be reached.

REFERENCES

Aradachi H, Honda K, Negoro H, Kubota T (1996) Median preoptic neurones projecting to the supraoptic nucleus are sensitive to haemodynamic changes as well as to rise in plasma osmolality in rats. J Neuroendocrinol 8:35–43.

Armstrong WE (1995) Morphological and electrophysiological classification of hypothalamic supraoptic neurons. Prog Neurobiol 47:291–339.

Bicknell RJ, Leng G (1983) Differential regulation of oxytocin- and vasopressin-secreting nerve terminals. Prog Brain Res 60:333–341.

Bourque CW (1989) Ionic basis for the intrinsic activation of rat supraoptic neurones by hyperosmotic stimuli. J Physiol (Lond) 417:263–277.

Bourque CW, Renaud LP (1990) Electrophysiology of mammalian magnocellular vasopressin and oxytocin neurosecretory neurons. Front Neuroendocrinol 11:183–212.

Bourque CW, Oliet SH, Richard D (1994) Osmoreceptors, osmoreception, and osmoregulation. Front Neuroendocrinol 15:231–274.

Brimble MJ, Dyball REJ (1977) Characterization of the responses of oxytocin- and vasopressin-secreting neurons in the supraoptic nucleus to osmotic stimulation. J Physiol (Lond) 271:253–271.

Conrad KP, Gellai M, North WG, Valtin H (1986) Influence of oxytocin on renal hemodynamics and electrolyte and water excretion. Am J Physiol 251:F290–F296.

Dyball RE, Leng G (1986) Regulation of the milk ejection reflex in the rat. J Physiol (Lond) 380:239–256.

Feng J, Brown B (1999) Coefficient of variation of interspike intervals greater than 0.5. How and when? Biol Cybern 80:291–297.

Glasgow E, Murase T, Zhang BJ, Verbalis JG, Gainer H (2000) Gene expression in the rat supraoptic nucleus induced by chronic hyperosmolality versus hypoosmolality. Am J Physiol 279:R1239–R1259.

Gutkowska J, Jankowski M, Lambert C, Mukaddam-Daher S, Zingg HH, McCann SM (1997) Oxytocin releases atrial natriuretic peptide by combining with oxytocin receptors in the heart. Proc Natl Acad Sci USA 94:11704–11709.

Higuchi T, Tadokoro Y, Hinda K, Negoro H (1986) Detailed analysis of blood oxytocin levels during suckling and parturition in the rat. J Endocrinol 110:251–256.

Ivanyi T, Dohanics J, Verbalis JG (1995) Effect of chronic hyponatremia on central and peripheral oxytocin and vasopressin secretion in rats. Neuroendocrinology 61:412–420.

Johnson AK (1985) The periventricular anteroventral third ventricle (AV3V): its relationship with the subfornical organ and neural systems involved in maintaining body fluid homeostasis. Brain Res Bull 15:595–601.

Leng G, Brown D (1997) The origins and significance of pulsatility in hormone secretion from the pituitary. J Neuroendocrinol 9:493–513.

Leng G, Dyball REJ (1991) Functional identification of magnocellular neuroendocrine neurones. In: Neuroendocrine research methods (Greenstein B, ed), pp 769–791. Chur, Switzerland: Harwood Academic.

Leng G, Mason WT, Dyer RG (1982) The supraoptic nucleus as an osmoreceptor. Neuroendocrinology 34:75–82.

Leng G, Blackburn RE, Dyball REJ, Russell JA (1989) The role of anterior peri-third ventricular structures in the regulation of supraoptic neuronal activity and neurohypophysial hormone secretion in the rat. J Neuroendocrinol 1:35–46.

Leng G, Way S, Dyball RE (1991) Identification of oxytocin cells in the rat supraoptic nucleus by their response to cholecystokinin injection. Neurosci Lett 122:159–162.

Leng G, Brown CH, Russell JA (1999) Physiological pathways regulating the activity of magnocellular neurosecretory cells. Prog Neurobiol 57:625–655.

Ludwig M, Leng G (1997) Autoinhibition of supraoptic nucleus vasopressin neurons in vivo - a combined retrodialysis/electrophysiological study in rats. Eur J Neurosci 9:2532–2540.

Ludwig M, Leng G (2000) GABAergic projection from the arcuate nucleus to the supraoptic nucleus in the rat. Neurosci Lett 281:195–197.

Mason WT (1980) Supraoptic neurones of the rat hypothalamus are osmosensitive. Nature 287:154–157.

McKinley MJ, Bicknell RJ, Hards D, McAllen RM, Vivas L (1992) Efferent neural pathways of the lamina terminalis subserving osmoregulation. Prog Brain Res 91:395–402.

Nissen R, Renaud LP (1994) GABA receptor mediation of median preoptic nucleus-evoked inhibition of supraoptic neurosecretory neurones in rat. J Physiol (Lond) 479:207–216.

Nissen R, Bourque CW, Renaud LP (1993) Membrane properties of organum vasculosum lamina terminalis neurons recorded in vitro. Am J Physiol 264:R811–R815.

Oliet SH, Bourque CW (1993) Mechanosensitive channels transduce osmosensitivity in supraoptic neurons. Nature 364:341–343.

Oliet SH, Bourque CW (1996) Gadolinium uncouples mechanical detection and osmoreceptor potential in supraoptic neurons. Neuron 16:175–181.

Randle JC, Bourque CW, Renaud LP (1986) Characterization of spontaneous and evoked inhibitory postsynaptic potentials in rat supraoptic neurosecretory neurons in vitro. J Neurophysiol 56:1703–1717.

Renaud LP, Tang M, McCann MJ, Stricker EM, Verbalis JG (1987) Cholecystokinin and gastric distension activate oxytocinergic cells in rat hypothalamus. Am J Physiol 253:R661–R665.

Richard D, Bourque CW (1995) Synaptic control of rat supraoptic neurones during osmotic stimulation of the organum vasculosum lamina terminalis in vitro. J Physiol (Lond) 489:567–577.

Shibuki K, Leng G, Way S (1988) Effects of naloxone and of intraperi-

toneal hypertonic saline upon oxytocin release and upon supraoptic neuronal activity. Neurosci Lett 88:75–80.
Sladek CD, Johnson AK (1983) Effect of anteroventral third ventricle lesions on vasopressin release by organ-cultured hypothalamo-neurohypophyseal explants. Neuroendocrinology 37:78–84.
Stricker EM, Verbalis JG (1986) Interaction of osmotic and volume stimuli in regulation of neurohypophysial secretion in rats. Am J Physiol 250:R267–R275.
Thrasher TN, Keil LC, Ramsay DJ (1982) Lesion of the organum vasculosum of the lamina terminalis (OVLT) attenuate osmotically-induced drinking and vasopressin secretion in the dog. Endocrinology 110:1837–1839.
Tuckwell HC (1988) Introduction to theoretical neurobiology, Vol 2. Cambridge, UK: Cambridge UP.
Verbalis JG (1984) An experimental model of syndrome of inappropriate antidiuretic hormone secretion in the rat. Am J Physiol 247:E540–E553.
Verbalis JG, Mangione MP, Stricker EM (1991) Oxytocin produces natriuresis in rats at physiological plasma concentrations. Endocrinology 128:1317–1322.
Voisin DL, Chakfe Y, Bourque CW (1999) Coincident detection of CSF Na+ and osmotic pressure in osmoregulatory neurons of the supraoptic nucleus. Neuron 24:453–460.
Yang CR, Senatorov VV, Renaud LP (1994) Organum vasculosum lamina terminalis-evoked postsynaptic responses in rat supraoptic neurones in vitro. J Physiol (Lond) 477:59–74.
Zhang BE, Glasgow E, Murase T, Verbalis JG, Gainer H (2001) Chronic hypoosmolality induces a selective decrease in magnocellular neurone soma and nuclear size in the rat hypothalamic supraoptic nucleus. J Neuroendocrinol 13:29–36.